Targeting IFN-λ Signaling Promotes Recovery from Central Nervous System Autoimmunity

Sindhu Manivasagam,*[,1] Jessica L. Williams,[†,1] Lauren L. Vollmer,* Bryan Bollman,[‡] Juliet M. Bartleson,[§] Shenjian Ai,* Gregory F. Wu,[‡,§] and Robyn S. Klein*[,‡,§]

Type III IFNs (IFNLs) are newly discovered cytokines, acting at epithelial and other barriers, that exert immunomodulatory functions in addition to their primary roles in antiviral defense. In this study, we define a role for IFNLs in maintaining autoreactive T cell effector function and limiting recovery in a murine model of multiple sclerosis (MS), experimental autoimmune encephalomyelitis. Genetic or Ab-based neutralization of the IFNL receptor (IFNLR) resulted in lack of disease maintenance during experimental autoimmune encephalomyelitis, with loss of CNS Th1 effector responses and limited axonal injury. Phenotypic effects of IFNLR signaling were traced to increased APC function, with associated increase in T cell production of IFN-γ and GM-CSF. Consistent with this, IFNL levels within lesions of CNS tissues derived from patients with MS were elevated compared with MS normal-appearing white matter. Furthermore, expression of IFNLR was selectively elevated in MS active lesions compared with inactive lesions or normal-appearing white matter. These findings suggest IFNL signaling as a potential therapeutic target to prevent chronic autoimmune neuroinflammation. ***The Journal of Immunology*****, 2022, 208: 1341–1351.**

Multiple sclerosis (MS) is a debilitating T cell–mediated, demyelinating autoimmune disease of the CNS (1) that progresses to severe disability in 90% of cases (2). Most patients with MS initially present with relapsing-remitting MS (RRMS), in which episodes of neurologic dysfunction are followed by partial or complete remission. Within 25 years, the majority of untreated patients with RRMS progress to secondary progressive MS (SPMS) and experience increasing neurologic deterioration (3). The Th1 cytokine IFN-γ and the Th17 cytokine IL-17 have demonstrated pathogenic roles in MS, whereas Th2 and regulatory T cells may limit disease activity (4, 5). Furthermore, Th cells producing GM-CSF have been recently identified to be expanded in the peripheral blood and cerebrospinal fluid of patients with RRMS (6). The strong role of T cells in MS is further underscored by the number of T cell–modulating therapies that have been successful for RRMS (7). However, currently approved immunomodulatory therapies are unable to prevent disease progression or promote recovery (8). Therefore, for patients with progressive disease, there are no treatments that prevent the chronic emergence of new disabilities or reverse deficits that previously developed. Studies indicate a critical role for CNS APCs, including dendritic cells (DCs), in disease progression via the initiation and maintenance of T cell autoreactivity (9–12). These studies used the established murine model for MS, experimental autoimmune encephalomyelitis (EAE), to define roles for classical $CD11c^{+}MHC^{+}$ DCs in Ag presentation and epitope spreading to myelin-specific $CD4^{+}$ T cells, which maintain disease. However, there are no therapies that specifically target these cell types or their cell-specific receptors.

Type III IFNs (IFNLs) or IFN-λs generate and sustain antiviral T cell responses via activation of its receptor, IFNLR, which is expressed by macrophages (13), subsets of DCs (14–17), and certain epithelial and endothelial barriers, including the blood–brain barrier (18). Type I and type III IFNs are closely related, signaling through common JAK-STAT signaling pathways that lead to transcription of IFN-stimulated genes (19–21). Specifically, type I IFN binds to the IFN-αβ receptor (IFNAR), and type III IFN binds to the heterodimeric receptor (IFNLR), which is comprised of two subunits, IFNLR1 and IL-10Rβ (22). As IFNAR is ubiquitously expressed, type I IFN inhibition of viral replication occurs in many cell types. In contrast, IFNLR-mediated antiviral responses exhibit specificity for viruses that replicate at barrier surfaces due to its cell-specific expression (21, 23). Studies in animal models of viral infections

*Department of Medicine, Washington University in St. Louis, St. Louis, MO; [†]Department of Neurosciences, Cleveland Clinic, Cleveland, OH; [‡]Department of Neurology, Washington University in St. Louis, St. Louis, MO; and [§]Department of Pathology and Immunology, Washington University in St. Louis, St. Louis, MO

[1]S.M. and J.L.W. made an equal contribution to this work.

ORCIDs: 0000-0002-9801-9580 (J.L.W.); 0000-0003-2342-1839 (J.M.B.); 0000-0002-9433-8939 (S.A.); 0000-0003-3588-0637 (G.F.W.).

Received for publication October 29, 2021. Accepted for publication January 7, 2022.

This work was supported by a postdoctoral fellowship from the National Multiple Sclerosis Society (to J.L.W.), National Institutes of Health/National Institute of Allergy and Infectious Diseases Grant K22AI125466 (to J.L.W.), the National Institutes of Health/National Institute of Neurological Disorders and Stroke Grants F31 NS108629-01A1 (to S.M.), P01 NS059560 (to R.S.K.), and R01 NS106289 (to G.F.W.), and research grants from the National Multiple Sclerosis Society (to R.S.K. and G.F.W.).

S.M., J.L.W., and R.S.K. were responsible for conceptualization; S.M., J.L.W., and R.S.K. designed the study methodology; S.M., J.L.W., L.L.V., and J.M.B. were responsible for analysis; S.M., J.L.W., L.L.V., B.B., J.M.B., and S.A. conducted the investigation; S.M. and J.L.W. wrote the original draft; S.M., J.L.W., G.F.W., and R.S.K. were responsible for review and editing of the manuscript; J.L.W. and R.S.K. performed supervision.

Address correspondence and reprint requests to Dr. Robyn S. Klein, Washington University School of Medicine, 660 S. Euclid Avenue, Campus Box 8051, St. Louis, MO 63110-1093. E-mail address: rklein@wustl.edu

The online version of this article contains supplemental material.

Abbreviations used in this article: anti-mIFNL2/3, neutralizing mAb that targets murine IFNL2 and IFNL3; DC, dendritic cell; dMBP, damaged myelin basic protein; EAE, experimental autoimmune encephalomyelitis; Iba1, ionized calcium binding adaptor molecule 1; IF, immunofluorescence; IFNAR, IFN-αβ receptor; IFNL, type III IFN; IFNLR, type III IFN receptor; LN, lymph node; MBP, myelin basic protein; MOG, myelin oligodendrocyte glycoprotein; MS, multiple sclerosis; NAWM, normal-appearing white matter; NIH, National Institutes of Health; qRT-PCR, quantitative RT-PCR; RORγt, retinoic acid–related orphan receptor γt; RRMS, relapsing-remitting multiple sclerosis; SMI-32, nonphosphorylated neurofilament H; SPMS, secondary progressive multiple sclerosis; WT, wild-type.

show that IFNL may act on DCs to modulate and augment downstream T cell polarization and effector function (15–17). Studies in tissues derived from patients with inflammatory disease or in murine models of these diseases indicate that IFNL contributes to inflammation and expansion of myeloid and T cell populations (24, 25), downregulates Th2 cytokines, and sustains Th1 activation (15, 26–28), including IFN-γ production (29). However, the cellular targets of IFNL and mechanisms for regulation of $CD4^+$ Th1 cell responses, especially in CNS autoimmune diseases, have not been defined.

In this study, we demonstrate that IFNL signaling sustains neuroinflammation in mice with EAE, a model of the human disease MS. Induction of CNS autoimmunity in EAE relies on peripheral priming of $CD4^+$ T cells, followed by local reactivation of effector myelin-specific T cells by CNS-resident and infiltrating APCs, including monocyte- and plasmacytoid-derived DCs (30–32) and B cells (33). Using murine models of EAE, we show that IFNL promotes disease maintenance and axonal injury through maintenance of effector Th1 cells within the CNS. Using global and cell-specific deletion strategies, we demonstrate that, in the presence of IFNL, APCs maintain costimulatory molecules that participate in $CD4^+$ T cell activation, with continued inflammatory cytokine production and disease maintenance. IFNL ligand and receptor levels are increased in lesions from patients with MS compared with MS normal-appearing white matter (NAWM) and non-MS CNS tissues. Importantly, targeting IFNL with a single-dose neutralizing strategy is sufficient to reverse clinical effects and prevent axonal injury, identifying a potential new therapeutic target to treat MS.

Materials and Methods

Animals

C57BL/6 (The Jackson Laboratory) and *Ifnlr1*$^{-/-}$ mice (Bristol-Myers Squibb) (18, 34) were maintained in specific pathogen-free conditions at Washington University in St. Louis. Littermate *Ifnlr1*$^{+/+}$, *Ifnlr1*$^{+/-}$, *Ifnlr1*$^{-/-}$ cohoused animals were bred and maintained in specific pathogen-free conditions at Washington University in St. Louis. *Ifnlr1*$^{fl/fl}$ CD11c-Cre and *Ifnlr1*$^{fl/fl}$ LysM-Cre lines were obtained from Dr. Megan Baldridge at Washington University in St. Louis) (35). All animal studies were performed in accordance with the Animal Care and Use Committee guidelines of the National Institutes of Health (NIH) and were conducted under protocols approved by the Animal Care and Use Committee of Washington University School of Medicine.

EAE induction

Active EAE was induced in 8–10-wk-old male and female mice by s.c. immunization with murine myelin oligodendrocyte glycoprotein $(MOG)_{35-55}$ peptide (GenScript) and CFA, as previously described (36). Pertussis toxin (400 ng/mouse; List Biological Laboratories) was administered i.p. on days 0 and 2 following immunization. Animals were monitored blindly for weight loss and clinical scores based on the following EAE scale: 1, tail weakness; 2, difficulty righting; 3, one hindlimb paralysis; 4, two hindlimb paralysis; and 5, moribund or dead. For adoptive transfer experiments, spleens from immunized animals were used to generated wild-type (WT) or *Ifnlr1*$^{-/-}$ MOG_{35-55}–specific Th1 clones, as previously described (37), and 10^7 cells were transferred to naive recipients via retro-orbital injection. The group size for EAE studies was determined on the basis of previous study reports and our past experience using this model.

Murine CNS tissue immunofluorescence

Frozen section preparation and detection of cell markers were accomplished as previously described (38). Briefly, mice were anesthetized and perfused with ice-cold Dulbecco's PBS, followed by 4% paraformaldehyde. Spinal cords were fixed overnight in 4% paraformaldehyde and then cryoprotected in 30% sucrose at 4°C for 72 h; sucrose was exchanged every 24 h during that time. Tissues were frozen in OCT (Thermo Fisher Scientific) and sectioned into 10-μm sections. Tissue sections were blocked with goat or donkey serum and 0.1% Triton X-100 (Sigma-Aldrich) for 1 h at room temperature. They were next exposed to anti-CD3 (1:200; catalog number 555273; BD Biosciences), –ionized calcium binding adaptor molecule 1 (Iba1) (1:250; catalog number 019-19741; Wako Chemicals), -MOG (1:80; AF2439; R&D Systems), –myelin basic protein (MBP) (1:100; ab40390; Abcam), –damaged MBP (dMBP) (1:2000; catalog number AB5864; Millipore), – nonphosphorylated neurofilament H (SMI-32) (1:1000; catalog number 801702; BioLegend), or -CD68 (1:500; catalog number MCA1957; Bio-Rad Laboratories) overnight at 4°C. Secondary Abs conjugated to Alexa Fluor 488, Alexa Fluor 555, or Alexa Fluor 647 (1:400; Invitrogen) were applied for 1 h at room temperature. Nuclei were counterstained with DAPI (Invitrogen). Coverslips were applied with ProLong Gold Antifade Mountant (Thermo Fisher Scientific).

TUNEL was performed on sections using the In Situ Cell Death Detection Kit, TMR Red (Millipore Sigma), according to the manufacturer's protocol. Immunofluorescent (IF) images were acquired using the ×20 or ×40 objective of a Zeiss LSM 880 confocal laser scanning microscope. The mean positive area was determined using appropriate isotype control Abs and quantified using Volocity (PerkinElmer) and Fiji (NIH) (39) image analysis software. Colocalization analysis was performed using Just Another Colocalization Plugin (JACoP) in Fiji.

In situ hybridization

Frozen sections were prepared as described under the murine CNS tissue IF section. Following sectioning of tissue, RNAscope 2.5 HD Duplex Assay (Advanced Cell Diagnostics) and RNAscope 2.5 HD Assay – Red (Advanced Cell Diagnostics) were performed as per the manufacturer's instructions. Probes (Advanced Cell Diagnostics) against *Ifnlr1* and CD11c (*Itgax*) were used. Following in situ hybridization, tissues were counterstained with 50% hematoxylin in water. Images were acquired using the ×20, ×40, or ×63 objective of a Zeiss Cell Observer Inverted Microscope.

CNS leukocyte isolation and flow cytometric analysis

Following cardiac perfusion with PBS, cells were isolated from the spleen, lymph nodes (LN), and spinal cords of WT or *Ifnlr1*$^{-/-}$ mice. Spleen and LN were pushed through a 70-μM strainer to create a single-cell suspension, following which cells from the spleen were incubated with ACK lysing buffer (Thermo Fisher Scientific). CNS tissue was digested in HBSS (Life Technologies) containing 0.05% collagenase D (Sigma-Aldrich), 0.1 μg/ml TLCK trypsin inhibitor (Sigma-Aldrich), 10 μg/ml DnaseI (Sigma-Aldrich) and 10 mM HEPES, pH 7.4 (Life Technologies) for 1 h at 37°C. Tissue was pushed through a 70-μM strainer to create a single-cell suspension and then centrifuged at 500 × *g* for 10 min. Cell pellets were resuspended in 37% Percoll (GE Healthcare) and centrifuged at 1200 × *g* for 30 min with deceleration set to 0 to remove myelin debris. Cell pellet was resuspended in PBS, counted using a hemocytometer, and stained at a concentration of 1:200 with fluorescently conjugated Abs. The following Abs were used: CD4 (clone RM4-5, catalog number 100527; BioLegend), GM-CSF (clone MP1-22E9, catalog number 505403; BioLegend), IFN-γ (clone XMG1.2, catalog number 505829; BioLegend), IL-17 (clone TC11-18H10.1, catalog number 506915; BioLegend), Tbet (clone 4B10, catalog number 561265; BD Biosciences), retinoic acid–related orphan receptor γt (RORγt) (clone Q31-378, catalog number 562683; BD Biosciences), CD44 (clone IM7, catalog number 103025; BioLegend), CD69 (clone H1.2F3, catalog number 104512; BioLegend), CD11b (clone M1/70, catalog number 557397; BD Biosciences), CD45 (clone 30-F11, catalog number 103113; BioLegend), CD11c (clone N418, catalog number 117333; BioLegend), CD86 (clone GL-1, catalog number 105026; BioLegend), and CD8 (clone 53-6.7, catalog number 100729; BioLegend) as previously described (40). The LIVE/DEAD Fixable Aqua Dead Cell Stain Kit (Thermo Fisher Scientific) was used to identify live cell populations. Data were collected using a Fortessa X-20 flow cytometer (BD Biosciences) or LSR-II flow cytometer (BD Biosciences) and analyzed using FlowJo software. Percentage data from flow cytometer were multiplied with hemocytometer cell counts to obtain a total number of cells per tissue.

In vivo administration of anti-IFNL2/3 neutralizing Ab

Mice used in the neutralization studies were randomly assigned to a treatment group on day 10 or day 14 post–Th1 cell transfer, anesthetized with 2% isoflurane, and administered either 100 μg of neutralizing mAb that targets murine IFNL2 and IFNL3 (anti-mIFNL2/3) or 100 μg mouse mAb specific for *Escherichia coli* β-galactosidase (InvivoGen) in 250 μl sterile PBS via retro-orbital injection. Clinical scores and weight loss were monitored blindly.

Postmortem human tissue IF analysis

Postmortem CNS tissue from non-MS controls and patients with clinically defined MS were obtained from the Neuroinflammatory Disease Tissue Repository at Washington University in St. Louis. Frozen sections were hydrated and blocked in 0.1% Triton X-100 and 10% donkey serum, followed by incubation with mouse anti-human CD31 (1:20; catalog number 550389; BD Biosciences) and goat anti-human IFNL (1:25; catalog number AF1587; R&D Systems) Abs. Secondary Abs conjugated to Alexa Fluor 488 or Alexa Fluor 555 (1:400; Molecular Probes) were applied for 1 h at

room temperature. Nuclei were counterstained with DAPI (Molecular Probes). IF images were acquired in a blinded manner using the ×20 or ×40 objective of a Zeiss LSM 880 confocal laser scanning microscope. The mean positive area was determined using appropriate isotype control Abs and quantified using Fiji (NIH) (39) image analysis software.

Quantitative RT-PCR

RNA was extracted using the RNeasy Micro Kit (Qiagen). RNA was treated with DNase, and cDNA was synthesized using MultiScribe reverse transcriptase (Applied Biosystems). Quantitative RT-PCR (qRT-PCR) was performed using Power SYBR Green PCR Master Mix (Thermo Fisher Scientific), primers [human *Ifnlr1* (41), human *Gapdh*, murine *Cxcl1*, murine *Cxcl9*, murine *Cxcl10*, and murine *Gapdh*], and CFX384 Touch Real-Time PCR Detection System (Bio-Rad Laboratories). Threshold cycle values >40 were not detected and therefore not quantified. The ΔΔ threshold cycle method was applied to determine differences in gene expression levels after normalization to *Gapdh*.

Statistical analyses

Data were analyzed using Prism 7.0 software (GraphPad). Clinical EAE data were analyzed by Mann–Whitney *U* test. Other experiments were analyzed with parametric tests (two-tailed Student *t* test or one- or two-way ANOVA), with correction for multiple comparisons where appropriate. Colocalization analysis was analyzed with Mander coefficients (M1 and M2) using Fiji software (NIH). A p value <0.05 was considered statistically significant. Samples were excluded only if determined to be a significant outlier, using Grubbs test with a significance level of $\alpha = 0.01$ (GraphPad). Data are expressed as means ± SEM. Sample sizes are indicated in the figure legends.

Data availability

The data from this study are tabulated in the main article and supplemental material. All reagents are available from R.S.K. under a material transfer agreement with Washington University. The data that support the findings of this study are also available from the corresponding author upon request.

Study approval

All animal experiments followed the guidelines approved by the Animal Care and Use Committee of Washington University School of Medicine. The use of the deidentified postmortem tissues obtained from a preexisting repository was not classified as human studies research, per Washington University's Institutional Review Board guidelines.

Results

Loss of IFNL signaling reduces severity of CNS autoimmune disease

To determine whether IFNL signaling impacts the induction of CNS autoimmunity, we induced EAE in WT and *Ifnlr1*$^{-/-}$ mice via active immunization with MOG_{35-55} peptide. Although the day of EAE onset was similar (Supplemental Fig. 1A), *Ifnlr1*$^{-/-}$ animals developed significantly less severe EAE compared with WT animals at peak disease and subsequently maintained lower clinical activity scores during recovery (Fig. 1A, Supplemental Fig. 1B). Consistent with the observed alterations in clinical disease course, areas containing Iba1-expressing myeloid cells within lumbar spinal cord lesions were significantly decreased in *Ifnlr1*$^{-/-}$ compared with WT mice at a chronic disease time point (day 27 postimmunization) (Fig. 1B). Importantly, *Ifnlr1*$^{-/-}$ animals also exhibited decreased area of axonal injury compared with WT animals, as assessed by IF detection of SMI-32 (Fig. 1B). No differences in levels of MBP, a protein found on the myelin sheath, or in damaged myelin basic protein (MBP_{69-86}, dMBP) (Supplemental Fig. 1C) were observed at this time point. These results are consistent with published studies demonstrating that axonal damage may not require prior demyelination (42) and suggest a critical role for IFNL in promoting inflammation and axonal injury during CNS autoimmune disease.

IFNL signaling does not alter peripheral immune responses after MOG_{35-55} peptide immunization

As baseline differences in peripheral immunity of WT and *Ifnlr1*$^{-/-}$ animals could underlie differences in disease expression within the CNS, we examined percentages and phenotypes of lymphoid cells

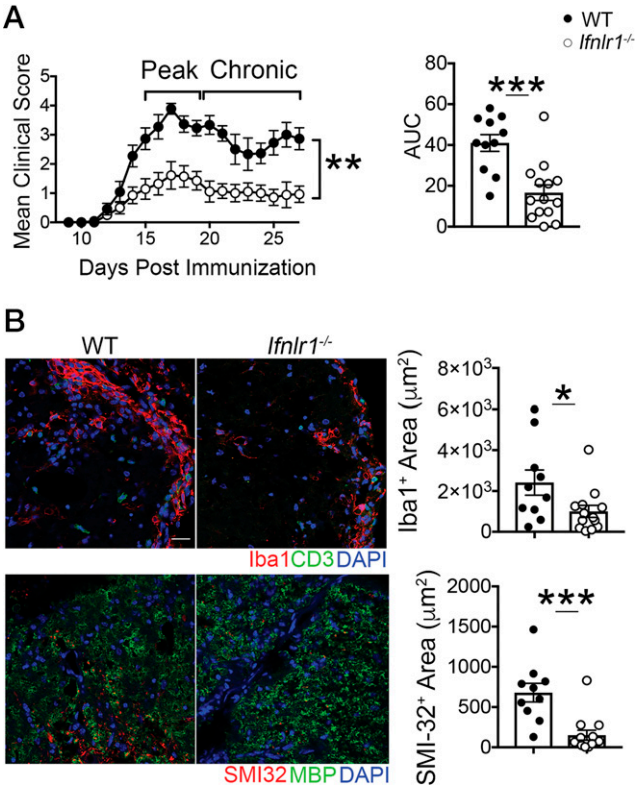

FIGURE 1. Loss of IFNL signaling reduces severity of CNS autoimmune disease. (**A**) EAE clinical course and area under the curve (AUC) analysis following active immunization with MOG_{35-55} peptide of WT and *Ifnlr1*$^{-/-}$ mice. Data are pooled from two independent experiments; $n = 11$ WT and $n = 14$ *Ifnlr1*$^{-/-}$ animals shown. (**B**) IF analysis of lesions within the ventral lumbar spinal cord of WT and *Ifnlr1*$^{-/-}$ mice during EAE at chronic time point indicated in (A). Iba1$^+$ and SMI-32$^+$ areas were quantified. Data are pooled from two independent experiments; $n = 10$ WT and $n = 14$ *Ifnlr1*$^{-/-}$ animals shown. Scale bar, 20 μm. Data are presented as means ± SEM. $*p < 0.05$, $**p < 0.01$, $***p < 0.001$ by Mann-Whitney *U* test (A) and two-tailed Student *t* test (A and B).

derived from the spleens and LN of naive WT and *Ifnlr1*$^{-/-}$ mice (Fig. 2A). Naive animals showed similar percentages of splenic and LN CD4$^+$, CD8$^+$, and CD19$^+$ cells in both genotypes (Fig. 2B). Analysis of peripheral lymphoid tissues 11 d following immunization with MOG_{35-55} also revealed no differences in percentages of CD4$^+$, CD8$^+$, and B220$^+$ cells nor in percentages of CD4$^+$ T cells expressing inflammatory cytokines or Th transcription factors (Fig. 2C). Upon in vitro restimulation with MOG_{35-55}, WT and *Ifnlr1*$^{-/-}$ CD4$^+$ Th1-polarized splenocytes and LN cells expressed similar levels of IFN-γ and GM-CSF (Fig. 2D), and induced EAE to a similar extent following adoptive transfer to naive WT recipients (Fig. 2E). Together, these data suggest that loss of IFNL signaling does not significantly alter the initial peripheral immune response to MOG_{35-55} immunization or the encephalitogenic capability of MOG_{35-55}–specific T cells during EAE induction.

IFNL signaling is required for the maintenance of autoimmune neuroinflammation

Because peripheral T cell activation did not differ between WT and *Ifnlr1*$^{-/-}$ animals, we examined whether IFNL signaling within the CNS differentially impacts T cell reactivation. Adoptive transfer of activated MOG_{35-55}–specific, Th1-polarized WT CD4$^+$ T cells into naive WT and *Ifnlr1*$^{-/-}$ recipients revealed no differences in time of EAE induction and peak clinical scores between the genotypes (Supplemental Fig. 2A). However, recovery of neurologic function

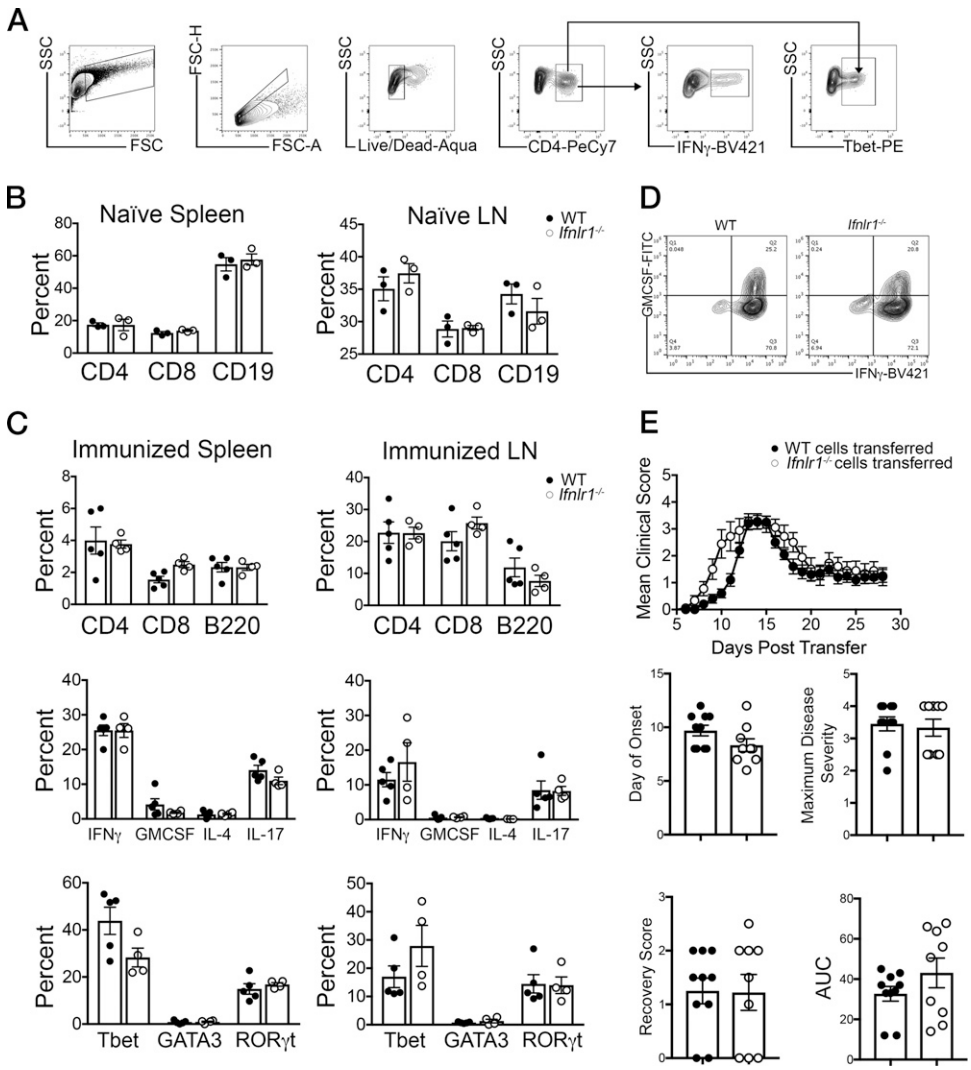

FIGURE 2. IFNL signaling does not alter peripheral T cell priming following immunization with MOG_{35-55} peptide. (**A**) Flow cytometric gating strategy. (**B**) Cells were isolated from spleens and LN of naive WT and *Ifnlr1*$^{-/-}$ animals. Percentage of $CD4^+$, $CD8^+$, and $CD19^+$ cells were gated and quantified from live cells. Data are representative of two independent experiments; $n = 3$/genotype shown. (**C**) WT and *Ifnlr1*$^{-/-}$ mice were actively immunized with MOG_{35-55} peptide. Cells were collected from spleen and draining LN 11 d following immunization. Flow cytometric analysis was performed on cells prior to stimulation to determine percentages of $CD4^+$, $CD8^+$, and $B220^+$ cells. $CD4^+$ cells were further gated on various cytokines and transcription factors; quantification is shown. Data are representative of two independent experiments; $n = 5$ WT and $n = 4$ *Ifnlr1*$^{-/-}$ animals shown. (**D**) Cells from (C) were stimulated and cultured in the presence of immunizing peptide and Th1-promoting cytokines with irradiated WT APCs. (D) After stimulation, MOG_{35-55}–specific WT and *Ifnlr1*$^{-/-}$ $CD4^+$ Th1 clones were analyzed for expression of GM-CSF and IFN-γ by flow cytometric analysis. (**E**) A total of 10^7 $CD4^+$ Th1 clones from (D) were injected retro-orbitally into naive WT recipients. EAE clinical course was monitored. Clinical onset of EAE, maximum disease score, score at recovery, and area under the curve (AUC) was quantified for each mouse. Data are pooled from two independent experiments; $n = 10$ animals with WT cells transferred and $n = 9$ animals with *Ifnlr1*$^{-/-}$ cells transferred. Data are presented as means ± SEM.

to baseline status occurred only in *Ifnlr1*$^{-/-}$ recipients (Fig. 3A). Correspondingly, lesion areas and axonal injury, assessed as in Fig. 1, were decreased, whereas levels of detection of MOG and dMBP were unaffected in *Ifnlr1*$^{-/-}$ compared with WT animals at a chronic disease time point (day 22 posttransfer) (Fig. 3B–D, Supplemental Fig. 2B). Analysis of infiltrating and activated resident myeloid cells via detection of Iba1, which participates in membrane ruffling and phagocytosis (43), revealed decreased expression of the phagocytic marker CD68 in *Ifnlr1*$^{-/-}$ spinal cords compared with WT at the same time point (Fig. 3C, 3D). To determine whether this decrease in $Iba1^+$ cells was due to baseline differences, we examined naive spinal cords and saw no differences in expression of Iba1 between WT and *Ifnlr1*$^{-/-}$ animals (Supplemental Fig. 3A). TUNEL assay analysis also demonstrated minimal colocalization with $Iba1^+$ cells in all groups (Supplemental Fig. 3B), suggesting differences in $Iba1^+$ expression and activation are not due to cell death. Overall, these data support the notion that IFNL signaling maintains inflammation in CNS lesions during autoimmunity.

To evaluate the therapeutic potential of targeting IFNL, we determined whether Ab neutralization recapitulates results observed in *Ifnlr1*$^{-/-}$ mice. Administration of neutralizing mAb that targets murine IFNL2 and IFNL3 (anti-mIFNL2/3) versus nonspecific IgG1 on day 10 following induction of EAE via adoptive transfer of MOG_{35-55}–specific $CD4^+$ T cells resulted in amelioration of peak EAE scores compared with controls (Fig. 3E). Similarly, single administration of anti-mIFNλ2/3 following peak EAE disease on day 14 post–cell transfer resulted in improved recovery from EAE (Fig. 3F) and decreased axonal injury (Fig. 3G). These studies not only validated data obtained through genetic approaches (Fig. 3A), but also suggest IFNL neutralization may be a therapeutic approach for reducing chronic neuroinflammation.

IFNL signaling promotes effector function of Th1 autoreactive cells within the inflamed CNS

The cytokines IFN-γ, GM-CSF, and IL-17, produced by effector $CD4^+$ T cells within the inflamed spinal cord, are strongly implicated in the induction and maintenance of EAE (44–46) and are elevated in postmortem brain samples from human patients with MS (47). Based on the crucial role of $CD4^+$ T cell cytokine production in disease expression, we determined whether IFNLR signaling impacts the effector function of infiltrating spinal cord $CD4^+$ T cells (Supplemental Fig. 4A). Despite transfer of equal numbers of MOG_{35-55}–specific WT Th1 cells, *Ifnlr1*$^{-/-}$ recipients exhibited reduced numbers of $CD4^+$ T cells within the spinal cord at peak disease compared with their WT counterparts (Fig. 4A, 4B). TUNEL assay analysis of spinal cords revealed increased $CD3^+$ T cell death in *Ifnlr1*$^{-/-}$ animals compared with WT animals (Fig. 4C), indicating IFNLR signaling may underlie T cell survival, and suggests a possible explanation for decreased T cell numbers. Examination of cytokine expression by spinal cord–infiltrating $CD4^+$ T cells at peak disease

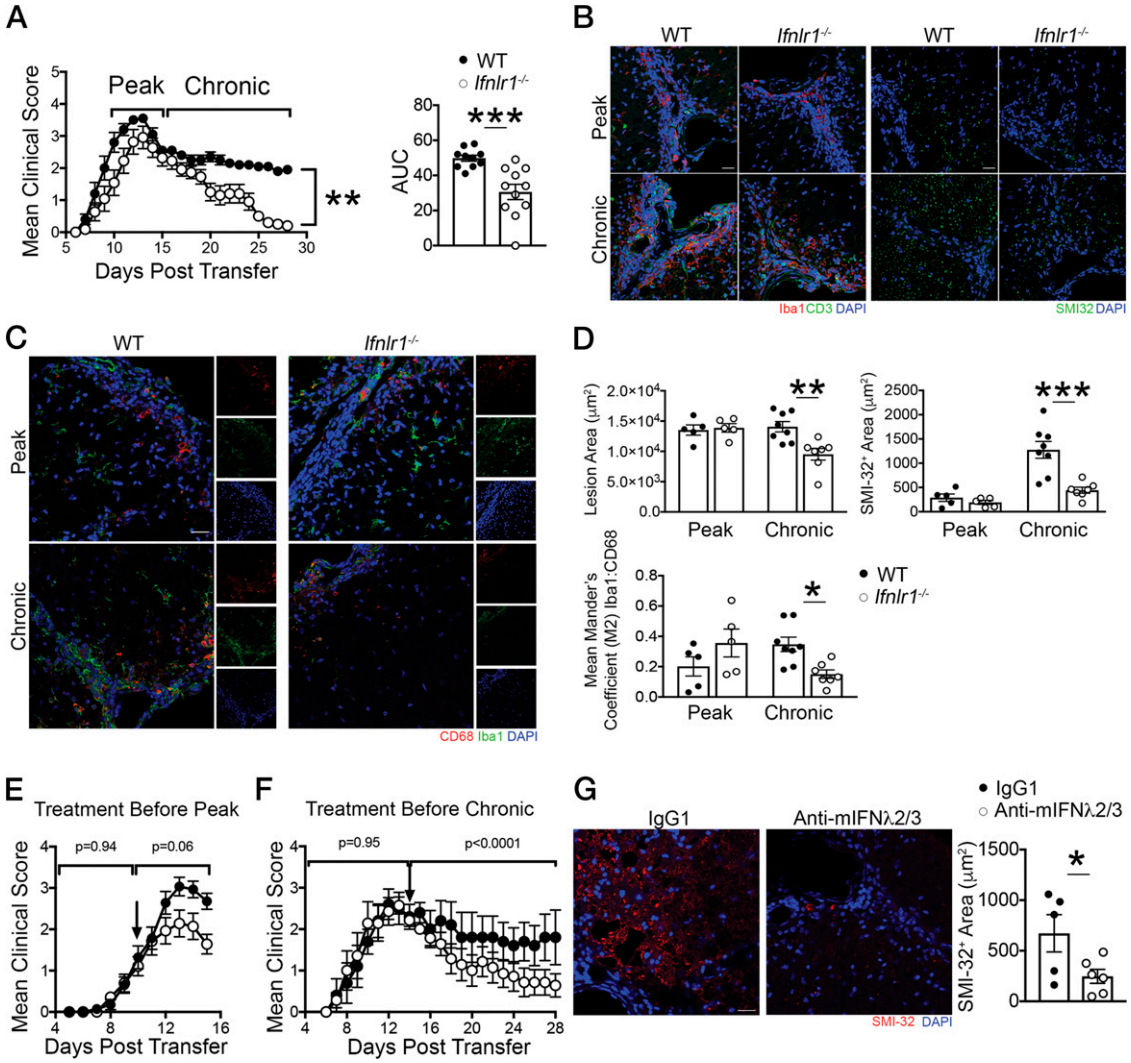

FIGURE 3. IFNL signaling is required for the maintenance of autoimmune neuroinflammation. (**A**) Activated MOG-specific Th1 clones were injected into naive WT or *Ifnlr1*$^{-/-}$ mice. Clinical course of recipient mice was monitored and area under the curve (AUC) was quantified. Data are representative of three independent experiments; $n = 10$ WT and $n = 11$ *Ifnlr1*$^{-/-}$ animals shown. (**B**–**D**) IF analysis and quantification of lesions within the ventral lumbar spinal cord of WT and *Ifnlr1*$^{-/-}$ mice at the time points indicated in (A). Lesion area was delineated using CD3 and Iba1 staining, and SMI-32^{+} area was quantified with comparisons between genotype. Mean Mander coefficient (M2) was used to quantify microglia and macrophage-associated CD68 staining. Data are representative of two independent experiments; $n = 5$ WT and $n = 5$ *Ifnlr1*$^{-/-}$ animals at peak time point and $n = 8$ WT and $n = 7$ *Ifnlr1*$^{-/-}$ animals at chronic time point. Scale bars, 20 μm. (**E**) Activated, MOG_{35-55}–specific WT Th1 clones were injected into naive WT recipients. On day 10 posttransfer, neutralizing mouse anti-mIFNL2/3 mAb (white circles) or an IgG1 control (black circles) was administered. Data are pooled from three independent experiments; $n = 14$ animals/group shown. (**F**) Activated, MOG_{35-55}-specific WT Th1 clones were injected into naive WT recipients. On day 14 posttransfer, neutralizing monoclonal mouse anti-mIFNL2/3 Ab (white circles) or an IgG1 control (black circles) was administered. Data are representative of three independent experiments; $n = 5$ IgG1 and $n = 7$ anti-mIFNL2/3 Ab animals shown. (**G**) SMI-32^{+} area was quantified in ventral lumbar spinal cords of animals from (F). Data shown for $n = 5$ IgG1 and $n = 6$ anti-mIFNL2/3 Ab animals. Scale bar, 20 μm. Data are presented as means ± SEM. $^{*}p < 0.05$, $^{**}p < 0.01$, $^{***}p < 0.001$ by Mann-Whitney *U* test (A, E, and F), two-tailed Student *t* test (A and G), and one-way ANOVA with multiple comparisons (D).

revealed that the majority expressed GM-CSF and IFN-γ, but not IL-17 (Fig. 4D, 4E). There were significantly fewer GM-CSF^{+} IFN-γ^{+}IL-17^{-}, GM-CSF^{-}IFN-γ^{+}IL-17^{-}, and GM-CSF^{-}IFN-γ^{+} IL-17^{+}CD4^{+} T cells in the spinal cords of *Ifnlr1*$^{-/-}$ compared with WT animals (Fig. 4E). Evaluation of CNS-derived CD4^{+} cells for expression of T cell transcription factors during peak EAE revealed decreased numbers of Tbet^{+}RORγt^{+}CD4^{+} cells in *Ifnlr1*$^{-/-}$ versus WT animals. Analysis of other populations showed an increase in Tbet^{-}RORγt^{+} CD4^{+} cells and a decrease in Tbet^{+}RORγt^{-} CD4^{+} T cells in *Ifnlr1*$^{-/-}$ versus WT animals (Fig. 4F). Analysis of T cell activation markers revealed decreased numbers of CD44^{+} and CD69^{+}CD4^{+} T cells derived from spinal cords of *Ifnlr1*$^{-/-}$ mice with EAE compared with similarly affected WT animals, suggesting IFNLR signaling is required for complete T cell effector function during EAE (Fig. 4G, Supplemental Fig. 4B). Overall, these data indicate that loss of IFNL signaling significantly diminishes numbers of activated, autoreactive Th1 cells, consistent with reduced disease expression observed in *Ifnlr1*$^{-/-}$ mice.

IFNL signaling promotes myeloid cell activation and chemokine expression within the CNS

As intrinsic IFNLR signaling did not affect T cell encephalitogenicity, we next examined the impact of IFNLR deficiency on the phenotypes and functions of CNS myeloid subsets during EAE (Supplemental Fig. 4A). We found that numbers of CD11b^{+} and CD11c^{+} cells derived from spinal cords of *Ifnlr1*$^{-/-}$ animals

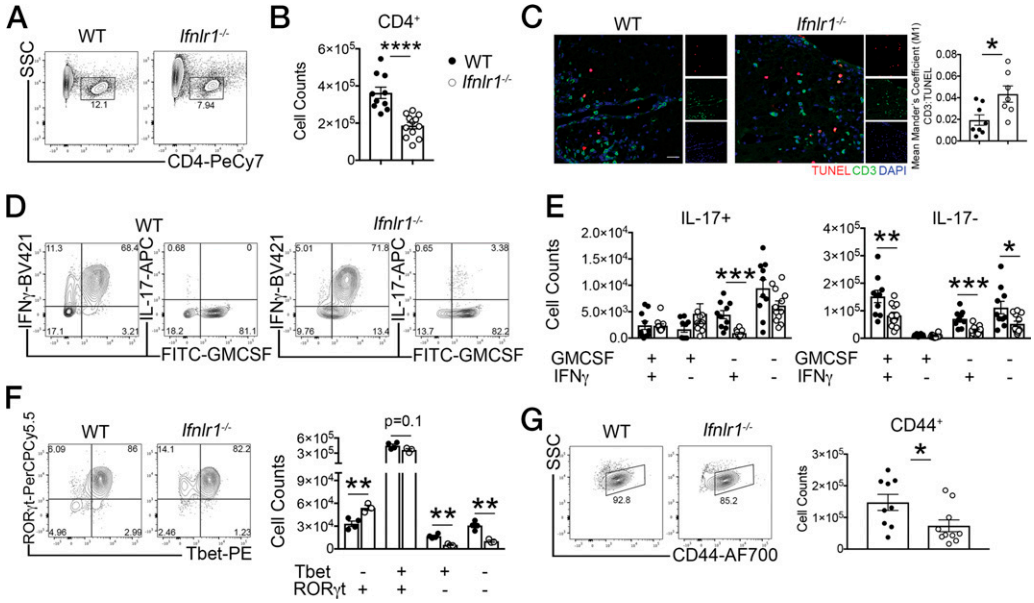

FIGURE 4. IFNL signaling maintains Th1 cell effector function during acute EAE. (**A** and **B**) Activated MOG-specific Th1 clones were injected into naive WT or *Ifnlr1*$^{-/-}$ mice. Flow cytometric analysis of infiltrating cells was performed on lumbar spinal cords during peak EAE (Fig. 2A). CD4$^+$ cells were identified from a live, single cell gate and quantified. Data are pooled from two independent experiments; $n = 10$ WT and $n = 12$ *Ifnlr1*$^{-/-}$ animals shown. (**C**) IF analysis of TUNEL$^+$ and CD3$^+$ colocalization in lumbar spinal cords at chronic EAE time point (Fig. 2A). Data shown for $n = 8$ WT and $n = 7$ *Ifnlr1*$^{-/-}$ animals. Scale bar, 20 μm. (**D** and **E**) Of the CD4$^+$ cells shown in (B), GM-CSF$^+$, IFN-γ$^+$, and IL-17$^+$ cells were identified and quantified. Data are pooled from two independent experiments; $n = 10$ WT and $n = 12$ *Ifnlr1*$^{-/-}$ animals shown. (**F**) CD4$^+$ cells were gated for Tbet and RORγt and quantified. Data are representative of two independent experiments; $n = 4$ WT and $n = 3$ *Ifnlr1*$^{-/-}$ animals shown. (**G**) CD4$^+$ cells were gated on CD44 and quantified. Data are pooled from two independent experiments; $n = 9$ WT and $n = 10$ *Ifnlr1*$^{-/-}$ animals shown. Data are presented as means ± SEM. *$p < 0.05$, **$p < 0.01$, ***$p < 0.001$, ****$p < 0.0001$ by two-tailed Student *t* test, comparing WT versus *Ifnlr1*$^{-/-}$.

compared with WT controls were significantly decreased (Fig. 5A). Within these populations, numbers of cells expressing costimulatory molecule CD86, which is required for effective local CD4$^+$ T cell reactivation during EAE, were also significantly decreased in *Ifnlr1*$^{-/-}$ versus WT mice (Fig. 5B). Furthermore, analysis of median fluorescence intensity of CD86 per cell revealed diminished expression in *Ifnlr1*$^{-/-}$ compared with WT in CD11b$^+$CD11c$^+$ and CD11b$^+$CD11c$^-$ populations (Fig. 5C). These data suggest that in the absence of IFNLR1, there are fewer activated APCs to provide the costimulatory signals necessary for proper T cell reactivation within the inflamed CNS.

In addition to providing costimulatory signals to T cells, myeloid cells may produce chemokines that influence recruitment of T cells to the CNS. We, therefore, examined whether presence of IFNL

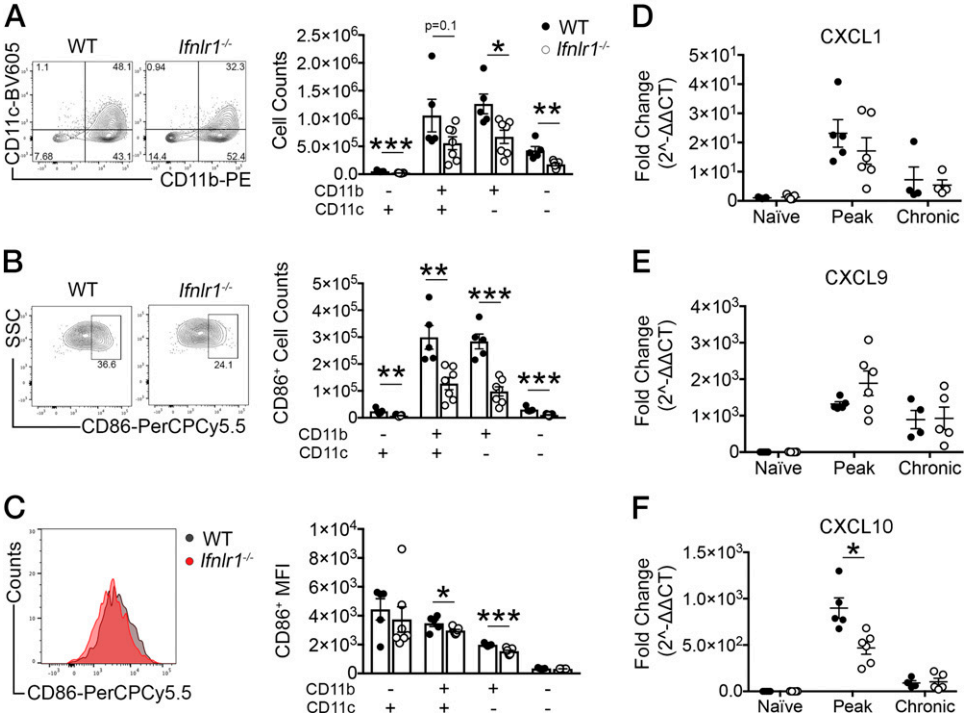

FIGURE 5. IFNL signaling maintains myeloid cells and CXCL10 expression in the CNS during acute EAE. (**A**) Live, single cells were gated on CD45, followed by CD11b and CD11c gating. Numbers of these populations were quantified. Each of these populations was analyzed for numbers of cells expressing CD86 (**B**) and median fluorescence intensity (MFI) of CD86 (**C**). Representative plots shown for the CD11b$^+$CD11c$^+$ population in (B) and (C). Data are shown for $n = 5$ WT and $n = 7$ *Ifnlr1*$^{-/-}$ animals. (**D**–**F**) RNA was isolated from spinal cords of WT and *Ifnlr1*$^{-/-}$ animals at three different time points during EAE disease course: naive, peak, and chronic. Expression of *Cxcl1* (D), *Cxcl9* (E), and *Cxcl10* (F) was quantified by qRT-PCR. Values shown as fold change ($2^{-\Delta\Delta Ct}$) compared with WT naive samples. Data are presented as means ± SEM. *$p < 0.05$, **$p < 0.01$, ***$p < 0.001$ by two-tailed Student *t* test (A–C) comparing WT versus *Ifnlr1*$^{-/-}$ and two-way ANOVA (D–F).

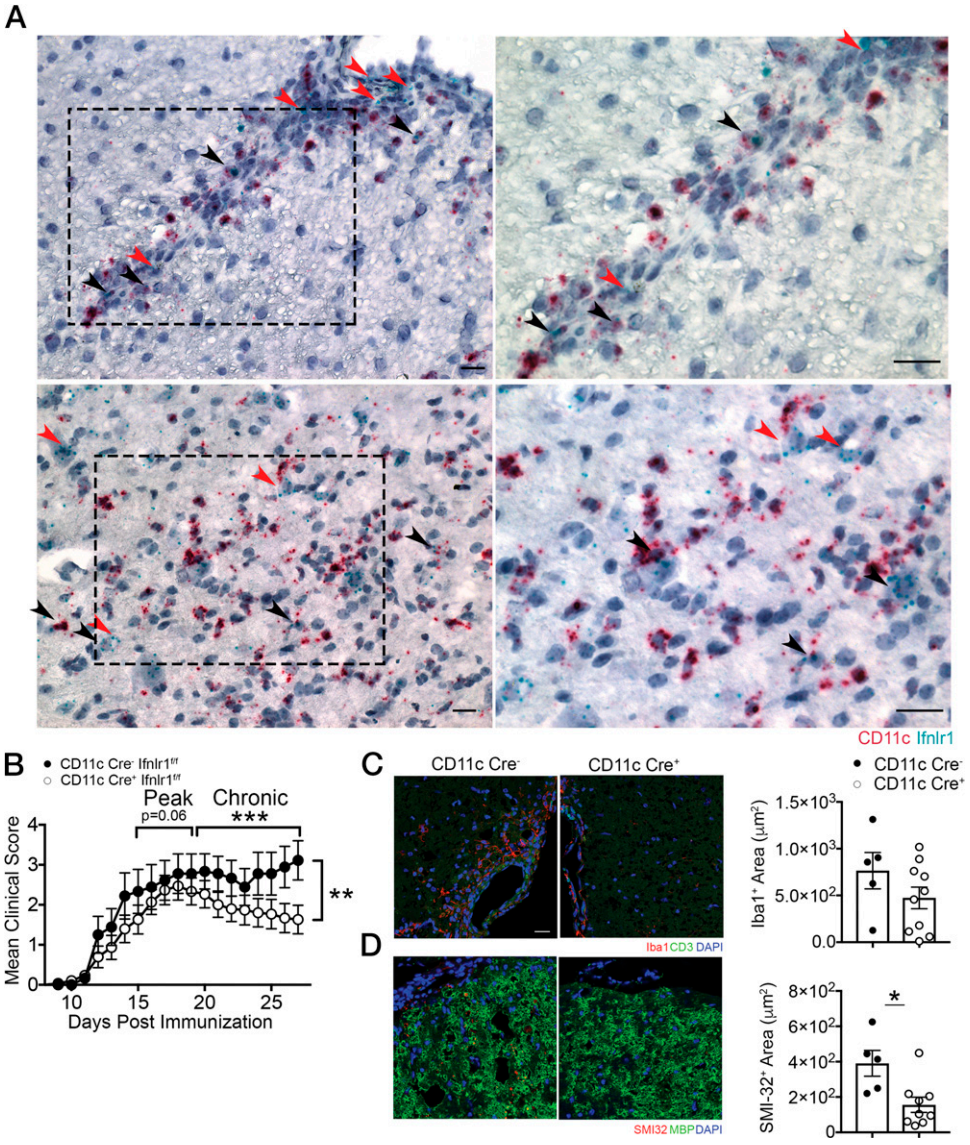

FIGURE 6. CD11c$^+$ cells are critical targets of IFNL during EAE. (**A**) Representative images of dual in situ hybridization for *Ifnlr1* and CD11c RNA on WT spinal cords collected at peak EAE. Black arrowheads demonstrate colocalization of *Ifnlr1* and *CD11c*. Red arrowheads depict *Ifnlr1*$^+$*CD11c*$^-$ cells. Images on right are magnified images of the field of view shown on the left. (**B**) *Ifnlr1*$^{fl/fl}$CD11c-Cre$^-$ and *Ifnlr1*$^{fl/fl}$ CD11c-Cre$^+$ mice were monitored for EAE disease course following active immunization. Data are pooled from three independent experiments; $n = 9$ *Ifnlr1*$^{fl/fl}$CD11c-Cre$^-$ and $n = 15$ *Ifnlr1*$^{fl/fl}$CD11c-Cre$^+$ animals shown. IF analysis of Iba1$^+$ (**C**) and SMI-32$^+$ area (**D**) in ventral lumbar spinal cord of *Ifnlr1*$^{fl/fl}$CD11c-Cre$^-$ and *Ifnlr1*$^{fl/fl}$ CD11c-Cre$^+$ mice at 27 d postimmunization. Scale bar, 20 μm. Data shown for $n = 5$ *Ifnlr1*$^{fl/fl}$CD11c-Cre$^-$ and $n = 10$ *Ifnlr1*$^{fl/fl}$CD11c-Cre$^+$ animals (C) and $n = 5$ *Ifnlr1*$^{fl/fl}$CD11c-Cre$^-$ and $n = 9$ *Ifnlr1*$^{fl/fl}$CD11c-Cre$^+$ animals (D). Data are presented as means ± SEM. $^*p < 0.05$, $^{**}p < 0.01$, $^{***}p < 0.001$ by Mann-Whitney *U* test (B) and two-tailed Student *t* test (C and D).

signaling altered expression of chemokines CXCL1, CXCL9, and CXCL10 that have been implicated in EAE pathogenesis (48, 49). We found increased spinal cord expression of CXCL10 during peak EAE in WT animals compared with *Ifnlr1*$^{-/-}$ animals, but no differences in CXCL1 and CXCL9 (Fig. 5D–F). These data suggest that IFNL may promote CXCL10-mediated recruitment of T cells to the CNS during EAE.

IFNL signals through CD11c$^+$ *cells to maintain neuroinflammation*

Consistent with prior studies detecting IFNLR expression by DCs (15, 17), *Ifnlr1* mRNA within spinal cords at peak EAE colocalized with CD11c mRNA within cells in perivascular lesions, as well as in the parenchyma (Fig. 6A). As shown previously (18), *Ifnlr1* mRNA expression was also detected in microvascular endothelial cells (Fig. 6A). Based on observed alterations in myeloid cell numbers in WT and *Ifnlr1*$^{-/-}$ animals (Fig. 5) and prior studies demonstrating both macrophages (13) and DCs (17) are IFNL targets, we determined the cell-specific effects of IFNL signaling in EAE via MOG_{35-55} peptide immunization of *Ifnlr1*$^{fl/fl}$CD11c-Cre (targeting DCs) (50) and *Ifnlr1*$^{fl/fl}$LysM-Cre (targeting neutrophils and macrophages) (51) animals. *Ifnlr1*$^{fl/fl}$CD11c-Cre$^+$ animals exhibited significant improvement of EAE scores in the chronic disease phase compared with *Ifnlr1*$^{fl/fl}$CD11c-Cre$^-$ animals (Fig. 6B), whereas no differences were observed between *Ifnlr1*$^{fl/fl}$LysM-Cre$^+$ and *Ifnlr1*$^{fl/fl}$ LysM-Cre$^-$ animals (Supplemental Fig. 4E). *Ifnlr1*$^{fl/fl}$CD11c-Cre$^+$ animals also exhibited significant decreases in axonal injury, but limited differences in Iba1$^+$ or MBP$^+$ cells compared with *Ifnlr1*$^{fl/fl}$ CD11c-Cre$^-$ animals (Fig. 6C, 6D, Supplemental Fig. 4F). These data suggest that IFNLR1 expression by CD11c$^+$ cells influences EAE disease course and neuropathology.

IFNL ligand and receptor levels are elevated in MS lesions

Given that IFNL signaling is critical for the maintenance of encephalomyelitis in mice, we wondered if IFNL expression differed within inflammatory demyelinating lesions versus NAWM within CNS tissues of patients with MS. Immunohistochemical detection of IFNL in human postmortem specimens derived from the brains of patients with no neurologic diseases (non-MS) and those with RRMS and SPMS (Fig. 7A, Table I) revealed similar levels in the NAWM of patients with MS and controls without MS. However, CNS lesions in tissues derived from patients with SPMS exhibited increased expression of IFNL compared with NAWM of patients with SPMS. There were no significant differences in level of IFNL expression between lesions of patients with RRMS and SPMS (Fig. 7B). In patients with RRMS, IFNL was localized to vessels, whereas in patients with SPMS, IFNL was also observed in parenchymal cells (Fig. 7A).

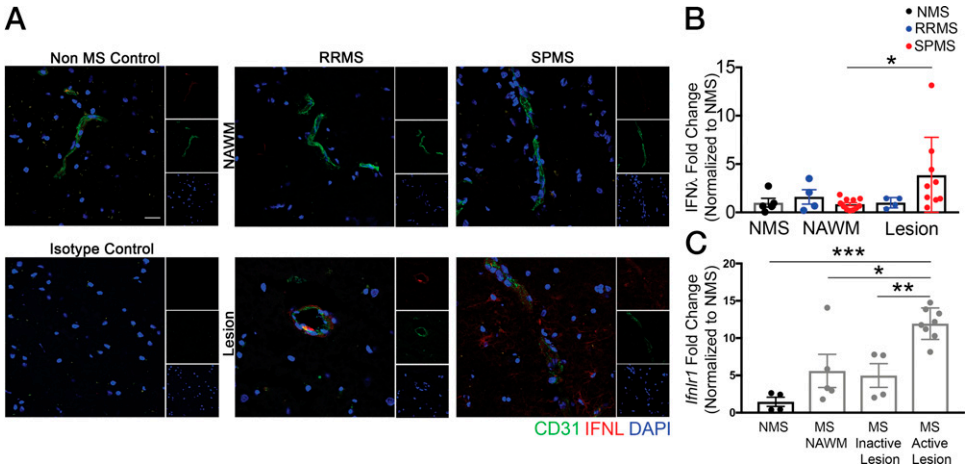

FIGURE 7. IFNL and IFNLR1 expression are increased in MS lesions. (**A**) Postmortem tissue specimens were analyzed: $n = 5$ samples from 5 non-MS (NMS) controls, $n = 4$ lesion samples and $n = 4$ NAWM samples from 3 RRMS patients, and $n = 9$ lesion samples and $n = 11$ NAWM samples from 7 SPMS patients (Table I). Samples from patients without MS were obtained from cortical white matter, whereas samples from patients with MS were obtained from multiple CNS regions, including the cortex, putamen, periventricular white matter, and midbrain. Perivascular and parenchymal localization of IFNL in NAWM and in lesions were visualized using IF for CD31 and IFNL. Nuclei were counterstained with DAPI. Scale bar, 20 μm. (**B**) Area of IFNL was quantified. All values were normalized to the average of the NMS samples; each data point represents one tissue sample. (**C**) RNA was analyzed from postmortem human specimens: $n = 4$ samples from 3 NMS controls and $n = 5$ NAWM samples, $n = 4$ inactive lesion samples, and $n = 8$ active lesion samples from 18 patients with MS (Table II). Relative *Ifnlr1* mRNA expression was measured by qRT-PCR. All values were normalized to the average of the NMS samples; each data point represents one tissue sample. Data are presented as means ± SEM. $*p < 0.05$, $**p < 0.01$, $***p < 0.001$ by one-way ANOVA with multiple comparisons (B and C).

qRT-PCR detection of *Ifnlr1* mRNA, within human postmortem CNS specimens derived from patients without MS and with MS (Table II), revealed significantly increased levels of *Ifnlr1* mRNA in active MS lesions, compared with non-MS tissue, MS NAWM, and MS-inactive lesions (Fig. 7C). These data, in conjunction with our murine findings, suggest IFNL signaling plays a critical role in promoting and maintaining inflammation within demyelinating lesions during CNS autoimmune disease.

Table I. Demographics of postmortem human samples for IF analysis

Sample	Lesion Classification	Age (y)	Sex	Disease Duration	PMI (h)	Cause of Death	MS Diagnosis	Tissue
1	—	69	F	—	43	Sepsis	—	Cerebrum
2	—	41	M	—	24	Cardiac arrest	—	Cerebrum
3	—	56	F	—	18	MI	—	Cerebrum
4	—	73	M	—	3	Cardiac arrest	—	Cerebrum
5	—	34	M	—	12	AML	—	Cerebrum
6	Inactive	41	F	15	12	Diabetes complication	RRMS	Cerebrum (PVWM)
7	NAWM							
8	Inactive	65	F	25	11	Lung cancer	RRMS	Cerebrum (PVWM)
9	NAWM							
10	Inactive	79	F	22	17	Pulmonary edema	RRMS	Cerebrum (PVWM)
11	NAWM							
12	Inactive							Cerebrum
13	NAWM							
14	Active	54	F	17	7	Pneumonia	SPMS	Putamen
15	NAWM							
16	Active							Cerebrum (cortex)
17	NAWM							
18	Active	50	F	13	20	Not reported	SPMS	Cerebrum (cortex)
19	NAWM							
20	Inactive	95	F	56	9	Pulmonary edema	SPMS	Cerebrum (cortex)
21	NAWM							
22	Inactive	70	M	20	8	Pneumonia	SPMS	Cerebrum (PVWM)
23	NAWM							
24	Active							Cerebrum (cortex)
25	NAWM							
26	NAWM	45	F	7	5	Respiratory failure	SPMS	Cerebrum (PVWM)
27	Active							Midbrain
28	NAWM							
29	Inactive	46	F	21	6	Pneumonia	SPMS	Midbrain
30	NAWM							
31	NAWM							Cerebrum
32	Inactive	50	F	12	16	PE	SPMS	Pons
33	NAWM							

AML, acute myelogenous leukemia; F, female; M, male; MI, myocardial infarction, PE, pulmonary embolism; PMI, postmortem interval; PVWM, periventricular white matter.

Table II. Demographics of postmortem human samples for qRT-PCR analysis

Sample	Lesion Classification	Age (y)	Sex	Disease Duration	PMI (h)	Cause of Death	MS Diagnosis	Tissue
1	—	69	F	—	43	Sepsis	—	Cerebrum
2	—	41	M	—	24	Cardiac arrest	—	Spinal cord
3	—	56	F	—	18	MI	—	Cerebrum
4	—							Spinal cord
5	NAWM	41	F	15	12	Diabetes complication	RRMS	Pons
6	Inactive	79	F	22	17	Pulmonary edema	RRMS	Cerebrum
7	NAWM							Spinal cord
8	Active	60	M	14	9	Respiratory failure	SPMS	Spinal cord
9	Active	54	F	22	8	Pneumonia	SPMS	Spinal cord
10	Active	50	F	13	20	Not reported	SPMS	Spinal cord
11	Inactive							Cerebrum (cortex)
12	NAWM	95	F	56	9	Pulmonary edema	SPMS	Pons
13	Active	54	F	17	7	Pneumonia	SPMS	Spinal cord
14	Inactive							Putamen
15	NAWM	77	F	Unknown	16	Not reported	SPMS	Spinal cord
16	Inactive	35	M	12	10	Not reported	PPMS	Spinal cord
17	Active	45	F	16	3	Pneumonia	PPMS	Cerebellum
18	Active						PPMS	Pons
19	Active	69	F	29	5	Colon cancer	PPMS	Medulla
20	Active						PPMS	Spinal cord
21	NAWM	86	F	31	12	Cardiac arrest	PPMS	Pons

F, female; M, male; MI, myocardial infarction; PMI, postmortem interval.

Discussion

The identification of new therapeutic targets is essential for the development of new drugs to prevent chronic disease in patients with MS. Our study identifies IFNL-IFNLR expression during CNS autoimmunity as a critical component in the maintenance and function of autoreactive T cells. Inactivation of IFNL signaling, via targeted deletion of *Ifnlr1*, led to reduced axonal pathology and recovery of neurologic function. These phenotypes correlated with reduced numbers of CNS-infiltrating T cells and myeloid cells. The effects of IFNLR1 signaling were T cell extrinsic, as in vitro–restimulated Th cells from WT and *Ifnlr1*$^{-/-}$ animals induced similar EAE following adoptive transfer into WT recipients. Instead, IFNL targeted myeloid cells, as CD11c^{+} cell–specific deletion of IFNLR1 improved recovery following EAE. IFNL ligand and receptor levels are also increased in lesions of patients with MS compared with NAWM. Importantly, neutralization of IFNL with a single administration of anti-mIFNλ2/3 Ab ameliorated peak disease and improved recovery when given before or after peak EAE, respectively. Overall, our study highlights IFNL as a potential therapeutic target to prevent chronic neuroinflammation.

In concordance with our findings, recent studies highlight that IFNL plays a significant role in immune-driven diseases. In a murine model of TLR7-induced lupus, IFNL promotes immune dysregulation through expansion of myeloid and T cell populations in the spleen and blood and induction of chemokine production by keratinocytes (24). Furthermore, IFNL protein levels are upregulated in patients with rheumatoid arthritis (52–55) and contribute to inflammation and cartilage degradation during osteoarthritis (25). Studies of allergic airway disease, vaccination-induced inflammation, and in vitro models examining T cell subtypes reveal the ability of IFNL to inhibit Th2 polarization (26–28, 56) and promote IFN-γ production (15, 27, 28, 57), indicating that IFNL may enhance Th1 function (58). The mechanisms by which IFNL alters T cell function are yet to be fully elucidated, but our data indicate that T cells are not directly targeted. Additionally, in corroboration with our work, studies of viral influenza suggest that IFNL modulation of CD11c^{+} DC responses affects the downstream adaptive immune response (17, 59). Conventional DCs may also produce IFNL to promote antitumor immunity via promotion of a Th1 microenvironment (60). One study has also indicated that IFNL may inhibit IL-17 responses (61), which may explain the increase in RORγt^{+} cells observed in *Ifnlr1*$^{-/-}$ animals compared with WT animals in the current study (Fig. 4F). As RORγt is a prototypical Th17 transcription factor, these data suggest that IFNL may influence Th17 cell function in addition to Th1 cells. IFNL may also influence Th2 cells in the CNS; however, we focused on Th1 and Th17 cells, as they have been strongly implicated in EAE pathogenesis (62). IFNL may also alter macrophage (13), NK cell (63), and neutrophil (61, 64, 65) polarization and cytokine production, as well as B cell differentiation (66).

IFNLs upregulate CXCL10 (24), leading to recruitment of T cells to sites of inflammation and maintenance of Th1 effector function. This may be due to the preferential expression of the CXCL10 receptor CXCR3 on Th1 cells compared with Th2 cells (67–69). Furthermore, DCs are key producers of CXCL10 and thus promote CXCL10-mediated Th1 effector function (70, 71). Taken together, this known interplay among CXCL10, DCs, and Th1 responses corroborates strongly with the data we present in this study. During CNS autoimmunity, IFNL may stimulate DCs to produce CXCL10 and thus increase numbers of Th1 effector cells within the spinal cord.

Examination of IFNL within the CNS has primarily been in the context of neuroinvasive viral illnesses. During West Nile virus encephalitis, IFNL substantially limits neuroinvasion by stabilizing the blood–brain barrier (18, 72). In our present work, lack of IFNL signaling reduces numbers of infiltrating T cells within the CNS and ameliorates EAE. These differences are likely because T cells and viruses use different mechanisms to enter the CNS. Although West Nile virus peripheral infection relies on blood–brain barrier disruption to cross into the CNS (73, 74), activated leukocytes are able to bind to adhesion molecules upregulated on the endothelium and extravasate in a transcellular fashion across the barrier (75). Aside from the endothelium, IFNL also acts on other CNS cell types; IFNL treatment of in vitro culture of primary astrocytes and neurons results in diminished replication of HSV type I within these cells (76). These studies focused on the effect of IFNL during acute viral infection, particularly on induction of JAK/STAT-mediated antiviral gene transcription and control of replication. Our findings suggest IFNL may have additional immunomodulatory roles within the CNS, especially in the context of ongoing inflammation. The role of IFNL in chronic neuroinvasive viral infection is unknown but may be similar to our observations, especially because IFNL has been shown to exert opposing effects on T cells based on viral chronicity in a model of lymphocytic choriomeningitis virus (77).

Nonredundant roles that distinguish IFNL functions from those of type I IFNs have undergone limited investigation. Models of

epithelial viral infections of lung and gut have shown temporal and spatial differences between type I and type III IFN responses (78, 79). One explanation for these differences is that whereas IFNAR is expressed ubiquitously, IFNLR is only expressed on a limited set of cells (80, 81). Our data also indicate that type I and type III IFN responses are quite distinct during CNS autoimmunity. Although we show that *Ifnlr1*$^{-/-}$ mice recover from EAE, *Ifnar1*$^{-/-}$ mice develop a more severe disease course, a phenotype mediated by IFNAR signaling in myeloid cells (82). Furthermore, type I IFN may skew the immune response away from Th1 and toward Th2 (83–85), whereas multiple studies, including ours, show that IFNLs promote Th1 polarization. This dichotomy demonstrates the protective function of type I IFN and inflammation-promoting properties of IFNLs during CNS autoimmunity.

Overall, our results highlight the important role that myeloid cells play in Th1 cell–mediated maintenance of neuroinflammation that requires IFNL signaling (86, 87). Furthermore, our Ab-mediated neutralization studies highlight the therapeutic potential of targeting IFNL because neutralization, even after establishment of encephalomyelitis, was significantly beneficial. Further studies identifying methods to reduce prolonged inflammation and damage in the CNS are necessary for developing therapeutics that prevent the chronic disease associated with MS.

Acknowledgments

We thank Dr. Angela Archambault for generating T cell lines that were used in adoptive transfer experiments (Washington University in St. Louis, St. Louis, MO). We also thank Dr. Anne H. Cross for providing MS tissue specimens and Dr. Robert Schmidt for pathological assessment of MS tissue (Washington University in St. Louis).

Disclosures

The authors have no financial conflicts of interest.

References

1. Reich, D. S., C. F. Lucchinetti, and P. A. Calabresi. 2018. Multiple sclerosis. *N. Engl. J. Med.* 378: 169–180.
2. Weinshenker, B. G., B. Bass, G. P. Rice, J. Noseworthy, W. Carriere, J. Baskerville, and G. C. Ebers. 1989. The natural history of multiple sclerosis: a geographically based study. I. Clinical course and disability. *Brain* 112: 133–146.
3. Lublin, F. D., S. C. Reingold, J. A. Cohen, G. R. Cutter, P. S. Sørensen, A. J. Thompson, J. S. Wolinsky, L. J. Balcer, B. Banwell, F. Barkhof, et al. 2014. Defining the clinical course of multiple sclerosis: the 2013 revisions. *Neurology* 83: 278–286.
4. Chitnis, T., and H. L. Weiner. 2017. CNS inflammation and neurodegeneration. *J. Clin. Invest.* 127: 3577–3587.
5. Dendrou, C. A., L. Fugger, and M. A. Friese. 2015. Immunopathology of multiple sclerosis. *Nat. Rev. Immunol.* 15: 545–558.
6. Galli, E., F. J. Hartmann, B. Schreiner, F. Ingelfinger, E. Arvaniti, M. Diebold, D. Mrdjen, F. van der Meer, C. Krieg, F. A. Nimer, et al. 2019. GM-CSF and CXCR4 define a T helper cell signature in multiple sclerosis. *Nat. Med.* 25: 1290–1300.
7. Wingerchuk, D. M., and J. L. Carter. 2014. Multiple sclerosis: current and emerging disease-modifying therapies and treatment strategies. *Mayo Clin. Proc.* 89: 225–240.
8. Baecher-Allan, C., B. J. Kaskow, and H. L. Weiner. 2018. Multiple sclerosis: mechanisms and immunotherapy. *Neuron* 97: 742–768.
9. Giles, D. A., P. C. Duncker, N. M. Wilkinson, J. M. Washnock-Schmid, and B. M. Segal. 2018. CNS-resident classical DCs play a critical role in CNS autoimmune disease. *J. Clin. Invest.* 128: 5322–5334.
10. Keller, C. W., C. Sina, M. B. Kotur, G. Ramelli, S. Mundt, I. Quast, L. A. Ligeon, P. Weber, B. Becher, C. Münz, and J. D. Lünemann. 2017. ATG-dependent phagocytosis in dendritic cells drives myelin-specific CD4^{+} T cell pathogenicity during CNS inflammation. *Proc. Natl. Acad. Sci. USA* 114: E11228–E11237.
11. Mundt, S., D. Mrdjen, S. G. Utz, M. Greter, B. Schreiner, and B. Becher. 2019. Conventional DCs sample and present myelin antigens in the healthy CNS and allow parenchymal T cell entry to initiate neuroinflammation. *Sci. Immunol.* 4: eaau8380.
12. Comabella, M., X. Montalban, C. Münz, and J. D. Lünemann. 2010. Targeting dendritic cells to treat multiple sclerosis. *Nat. Rev. Neurol.* 6: 499–507.
13. Read, S. A., R. Wijaya, M. Ramezani-Moghadam, E. Tay, S. Schibeci, C. Liddle, V. W. T. Lam, L. Yuen, M. W. Douglas, D. Booth, et al. 2019. Macrophage coordination of the interferon lambda immune response. *Front. Immunol.* 10: 2674.
14. Yin, Z., J. Dai, J. Deng, F. Sheikh, M. Natalia, T. Shih, A. Lewis-Antes, S. B. Amrute, U. Garrigues, S. Doyle, et al. 2012. Type III IFNs are produced by and stimulate human plasmacytoid dendritic cells. *J. Immunol.* 189: 2735–2745.
15. Koltsida, O., M. Hausding, A. Stavropoulos, S. Koch, G. Tzelepis, C. Ubel, S. V. Kotenko, P. Sideras, H. A. Lehr, M. Tepe, et al. 2011. IL-28A (IFN-λ2) modulates lung DC function to promote Th1 immune skewing and suppress allergic airway disease. *EMBO Mol. Med.* 3: 348–361.
16. Dolganiuc, A., K. Kodys, C. Marshall, B. Saha, S. Zhang, S. Bala, and G. Szabo. 2012. Type III interferons, IL-28 and IL-29, are increased in chronic HCV infection and induce myeloid dendritic cell-mediated FoxP3+ regulatory T cells. *PLoS One* 7: e44915.
17. Hemann, E. A., R. Green, J. B. Turnbull, R. A. Langlois, R. Savan, and M. Gale, Jr. 2019. Interferon-λ modulates dendritic cells to facilitate T cell immunity during infection with influenza A virus. *Nat. Immunol.* 20: 1035–1045.
18. Lazear, H. M., B. P. Daniels, A. K. Pinto, A. C. Huang, S. C. Vick, S. E. Doyle, M. Gale, Jr., R. S. Klein, and M. S. Diamond. 2015. Interferon-λ restricts West Nile virus neuroinvasion by tightening the blood-brain barrier. *Sci. Transl. Med.* 7: 284ra59.
19. Lazear, H. M., T. J. Nice, and M. S. Diamond. 2015. Interferon-λ: immune functions at barrier surfaces and beyond. *Immunity* 43: 15–28.
20. Syedbasha, M., and A. Egli. 2017. Interferon lambda: modulating immunity in infectious Diseases. *Front. Immunol.* 8: 119.
21. Wells, A. I., and C. B. Coyne. 2018. Type III interferons in antiviral defenses at barrier surfaces. *Trends Immunol.* 39: 848–858.
22. Sheppard, P., W. Kindsvogel, W. Xu, K. Henderson, S. Schlutsmeyer, T. E. Whitmore, R. Kuestner, U. Garrigues, C. Birks, J. Roraback, et al. 2003. IL-28, IL-29 and their class II cytokine receptor IL-28R. *Nat. Immunol.* 4: 63–68.
23. Sommereyns, C., S. Paul, P. Staeheli, and T. Michiels. 2008. IFN-lambda (IFN-lambda) is expressed in a tissue-dependent fashion and primarily acts on epithelial cells in vivo. *PLoS Pathog.* 4: e1000017.
24. Goel, R. R., X. Wang, L. J. O'Neil, S. Nakabo, K. Hasneen, S. Gupta, G. Wigerblad, L. P. Blanco, J. B. Kopp, M. I. Morasso, et al. 2020. Interferon lambda promotes immune dysregulation and tissue inflammation in TLR7-induced lupus. *Proc. Natl. Acad. Sci. USA* 117: 5409–5419.
25. Xu, L., Q. Peng, W. Xuan, X. Feng, X. Kong, M. Zhang, W. Tan, M. Xue, and F. Wang. 2016. Interleukin-29 enhances synovial inflammation and cartilage degradation in osteoarthritis. *Mediators Inflamm.* 2016: 9631510.
26. Won, J., C. H. Gil, A. Jo, and H. J. Kim. 2019. Inhaled delivery of interferon-lambda restricts epithelial-derived Th2 inflammation in allergic asthma. *Cytokine* 119: 32–36.
27. Dai, J., N. J. Megjugorac, G. E. Gallagher, R. Y. Yu, and G. Gallagher. 2009. IFN-lambda1 (IL-29) inhibits GATA3 expression and suppresses Th2 responses in human naive and memory T cells. *Blood* 113: 5829–5838.
28. Jordan, W. J., J. Eskdale, S. Srinivas, V. Pekarek, D. Kelner, M. Rodia, and G. Gallagher. 2007. Human interferon lambda-1 (IFN-lambda1/IL-29) modulates the Th1/Th2 response. *Genes Immun.* 8: 254–261.
29. de Groen, R. A., A. Boltjes, J. Hou, B. S. Liu, F. McPhee, J. Friborg, H. L. Janssen, and A. Boonstra. 2015. IFN-λ-mediated IL-12 production in macrophages induces IFN-γ production in human NK cells. *Eur. J. Immunol.* 45: 250–259.
30. Greter, M., F. L. Heppner, M. P. Lemos, B. M. Odermatt, N. Goebels, T. Laufer, R. J. Noelle, and B. Becher. 2005. Dendritic cells permit immune invasion of the CNS in an animal model of multiple sclerosis. *Nat. Med.* 11: 328–334.
31. Simpson, J. E., J. Newcombe, M. L. Cuzner, and M. N. Woodroofe. 1998. Expression of monocyte chemoattractant protein-1 and other beta-chemokines by resident glia and inflammatory cells in multiple sclerosis lesions. *J. Neuroimmunol.* 84: 238–249.
32. Windhagen, A., J. Newcombe, F. Dangond, C. Strand, M. N. Woodroofe, M. L. Cuzner, and D. A. Hafler. 1995. Expression of costimulatory molecules B7-1 (CD80), B7-2 (CD86), and interleukin 12 cytokine in multiple sclerosis lesions. *J. Exp. Med.* 182: 1985–1996.
33. Parker Harp, C. R., A. S. Archambault, J. Sim, S. T. Ferris, R. J. Mikesell, P. A. Koni, M. Shimoda, C. Linington, J. H. Russell, and G. F. Wu. 2015. B cell antigen presentation is sufficient to drive neuroinflammation in an animal model of multiple sclerosis. *J. Immunol.* 194: 5077–5084.
34. Ank, N., M. B. Iversen, C. Bartholdy, P. Staeheli, R. Hartmann, U. B. Jensen, F. Dagnaes-Hansen, A. R. Thomsen, Z. Chen, H. Haugen, et al. 2008. An important role for type III interferon (IFN-lambda/IL-28) in TLR-induced antiviral activity. *J. Immunol.* 180: 2474–2485.
35. Baldridge, M. T., S. Lee, J. J. Brown, N. McAllister, K. Urbanek, T. S. Dermody, T. J. Nice, and H. W. Virgin. 2017. Expression of *Ifnlr1* on intestinal epithelial cells is critical to the antiviral effects of interferon lambda against norovirus and reovirus. *J. Virol.* 91: e02079-16.
36. Cruz-Orengo, L., Y. J. Chen, J. H. Kim, D. Dorsey, S. K. Song, and R. S. Klein. 2011. CXCR7 antagonism prevents axonal injury during experimental autoimmune encephalomyelitis as revealed by in vivo axial diffusivity. *J. Neuroinflammation* 8: 170.
37. Lees, J. R., P. T. Golumbek, J. Sim, D. Dorsey, and J. H. Russell. 2008. Regional CNS responses to IFN-gamma determine lesion localization patterns during EAE pathogenesis. *J. Exp. Med.* 205: 2633–2642.
38. Williams, J. L., J. R. Patel, B. P. Daniels, and R. S. Klein. 2014. Targeting CXCR7/ACKR3 as a therapeutic strategy to promote remyelination in the adult central nervous system. *J. Exp. Med.* 211: 791–799.

39. Schindelin, J., I. Arganda-Carreras, E. Frise, V. Kaynig, M. Longair, T. Pietzsch, S. Preibisch, C. Rueden, S. Saalfeld, B. Schmid, et al. 2012. Fiji: an open-source platform for biological-image analysis. *Nat. Methods* 9: 676–682.
40. McCandless, E. E., Q. Wang, B. M. Woerner, J. M. Harper, and R. S. Klein. 2006. CXCL12 limits inflammation by localizing mononuclear infiltrates to the perivascular space during experimental autoimmune encephalomyelitis. *J. Immunol.* 177: 8053–8064.
41. Duong, F. H., G. Trincucci, T. Boldanova, D. Calabrese, B. Campana, I. Krol, S. C. Durand, L. Heydmann, M. B. Zeisel, T. F. Baumert, and M. H. Heim. 2014. IFN-λ receptor 1 expression is induced in chronic hepatitis C and correlates with the IFN-λ3 genotype and with nonresponsiveness to IFN-α therapies. *J. Exp. Med.* 211: 857–868.
42. Nikić, I., D. Merkler, C. Sorbara, M. Brinkoetter, M. Kreutzfeldt, F. M. Bareyre, W. Brück, D. Bishop, T. Misgeld, and M. Kerschensteiner. 2011. A reversible form of axon damage in experimental autoimmune encephalomyelitis and multiple sclerosis. *Nat. Med.* 17: 495–499.
43. Ohsawa, K., Y. Imai, H. Kanazawa, Y. Sasaki, and S. Kohsaka. 2000. Involvement of Iba1 in membrane ruffling and phagocytosis of macrophages/microglia. *J. Cell Sci.* 113: 3073–3084.
44. Komiyama, Y., S. Nakae, T. Matsuki, A. Nambu, H. Ishigame, S. Kakuta, K. Sudo, and Y. Iwakura. 2006. IL-17 plays an important role in the development of experimental autoimmune encephalomyelitis. *J. Immunol.* 177: 566–573.
45. Codarri, L., G. Gyülvészi, V. Tosevski, L. Hesske, A. Fontana, L. Magnenat, T. Suter, and B. Becher. 2011. RORγt drives production of the cytokine GM-CSF in helper T cells, which is essential for the effector phase of autoimmune neuroinflammation. *Nat. Immunol.* 12: 560–567.
46. El-Behi, M., B. Ciric, H. Dai, Y. Yan, M. Cullimore, F. Safavi, G. X. Zhang, B. N. Dittel, and A. Rostami. 2011. The encephalitogenicity of T(H)17 cells is dependent on IL-1- and IL-23-induced production of the cytokine GM-CSF. *Nat. Immunol.* 12: 568–575.
47. Rasouli, J., B. Ciric, J. Imitola, P. Gonnella, D. Hwang, K. Mahajan, E. R. Mari, F. Safavi, T. P. Leist, G. X. Zhang, and A. Rostami. 2015. Expression of GM-CSF in T cells is increased in multiple aclerosis and auppressed by IFN-β therapy. *J. Immunol.* 194: 5085–5093.
48. Carter, S. L., M. Müller, P. M. Manders, and I. L. Campbell. 2007. Induction of the genes for Cxcl9 and Cxcl10 is dependent on IFN-gamma but shows differential cellular expression in experimental autoimmune encephalomyelitis and by astrocytes and microglia in vitro. *Glia* 55: 1728–1739.
49. Omari, K. M., S. E. Lutz, L. Santambrogio, S. A. Lira, and C. S. Raine. 2009. Neuroprotection and remyelination after autoimmune demyelination in mice that inducibly overexpress CXCL1. *Am. J. Pathol.* 174: 164–176.
50. Caton, M. L., M. R. Smith-Raska, and B. Reizis. 2007. Notch-RBP-J signaling controls the homeostasis of CD8- dendritic cells in the spleen. *J. Exp. Med.* 204: 1653–1664.
51. Clausen, B. E., C. Burkhardt, W. Reith, R. Renkawitz, and I. Förster. 1999. Conditional gene targeting in macrophages and granulocytes using LysMcre mice. *Transgenic Res.* 8: 265–277.
52. Wang, F., L. Xu, X. Feng, D. Guo, W. Tan, and M. Zhang. 2012. Interleukin-29 modulates proinflammatory cytokine production in synovial inflammation of rheumatoid arthritis. *Arthritis Res. Ther.* 14: R228.
53. Wu, Q., Q. Yang, H. Sun, M. Li, Y. Zhang, and A. La Cava. 2013. Serum IFN-λ1 is abnormally elevated in rheumatoid arthritis patients. *Autoimmunity* 46: 40–43.
54. Castillo-Martínez, D., M. Juarez, M. Patlán, A. Páez, F. Massó, and L. M. Amezcua-Guerra. 2017. Type-III interferons and rheumatoid arthritis: correlation between interferon lambda 1 (interleukin 29) and antimutated citrullinated vimentin antibody levels. *Autoimmunity* 50: 82–85.
55. Chang, Q. J., C. Lv, F. Zhao, T. S. Xu, and P. Li. 2017. Elevated serum levels of interleukin-29 are associated with disease activity in rheumatoid arthritis patients with anti-cyclic citrullinated peptide antibodies. *Tohoku J. Exp. Med.* 241: 89–95.
56. Srinivas, S., J. Dai, J. Eskdale, G. E. Gallagher, N. J. Megjugorac, and G. Gallagher. 2008. Interferon-lambda1 (interleukin-29) preferentially down-regulates interleukin-13 over other T helper type 2 cytokine responses in vitro. *Immunology* 125: 492–502.
57. Morrow, M. P., J. Yan, P. Pankhong, B. Ferraro, M. G. Lewis, A. S. Khan, N. Y. Sardesai, and D. B. Weiner. 2010. Unique Th1/Th2 phenotypes induced during priming and memory phases by use of interleukin-12 (IL-12) or IL-28B vaccine adjuvants in rhesus macaques. *Clin. Vaccine Immunol.* 17: 1493–1499.
58. Egli, A., D. M. Santer, D. O'Shea, D. L. Tyrrell, and M. Houghton. 2014. The impact of the interferon-lambda family on the innate and adaptive immune response to viral infections. *Emerg. Microbes Infect.* 3: e51.
59. Ye, L., D. Schnepf, J. Becker, K. Ebert, Y. Tanriver, V. Bernasconi, H. H. Gad, R. Hartmann, N. Lycke, and P. Staeheli. 2019. Interferon-λ enhances adaptive mucosal immunity by boosting release of thymic stromal lymphopoietin. *Nat. Immunol.* 20: 593–601.
60. Hubert, M., E. Gobbini, C. Couillault, T. V. Manh, A. C. Doffin, J. Berthet, C. Rodriguez, V. Ollion, J. Kielbassa, C. Sajous, et al. 2020. IFN-III is selectively produced by cDC1 and predicts good clinical outcome in breast cancer. *Sci. Immunol.* 5: eaav3942.
61. Blazek, K., H. L. Eames, M. Weiss, A. J. Byrne, D. Perocheau, J. E. Pease, S. Doyle, F. McCann, R. O. Williams, and I. A. Udalova. 2015. IFN-λ resolves inflammation via suppression of neutrophil infiltration and IL-1β production. *J. Exp. Med.* 212: 845–853.
62. Jäger, A., V. Dardalhon, R. A. Sobel, E. Bettelli, and V. K. Kuchroo. 2009. Th1, Th17, and Th9 effector cells induce experimental autoimmune encephalomyelitis with different pathological phenotypes. *J. Immunol.* 183: 7169–7177.
63. Gimeno Brias, S., M. Marsden, J. Forbester, M. Clement, C. Brandt, K. Harcourt, L. Kane, L. Chapman, S. Clare, and I. R. Humphreys. 2018. Interferon lambda is required for interferon gamma-expressing NK cell responses but does not afford antiviral protection during acute and persistent murine cytomegalovirus infection. *PLoS One* 13: e0197596.
64. Broggi, A., Y. Tan, F. Granucci, and I. Zanoni. 2017. IFN-λ suppresses intestinal inflammation by non-translational regulation of neutrophil function. *Nat. Immunol.* 18: 1084–1093.
65. Espinosa, V., O. Dutta, C. McElrath, P. Du, Y. J. Chang, B. Cicciarelli, A. Pitler, I. Whitehead, J. J. Obar, J. E. Durbin, et al. 2017. Type III interferon is a critical regulator of innate antifungal immunity. *Sci. Immunol.* 2: eaan5357.
66. Syedbasha, M., F. Bonfiglio, J. Linnik, C. Stuehler, D. Wüthrich, and A. Egli. 2020. Interferon-λ enhances the differentiation of naive B cells into pasmablasts via the mTORC1 pathway. *Cell Rep.* 33: 108211.
67. Dufour, J. H., M. Dziejman, M. T. Liu, J. H. Leung, T. E. Lane, and A. D. Luster. 2002. IFN-gamma-inducible protein 10 (IP-10; CXCL10)-deficient mice reveal a role for IP-10 in effector T cell generation and trafficking. *J. Immunol.* 168: 3195–3204.
68. Vasquez, R. E., L. Xin, and L. Soong. 2008. Effects of CXCL10 on dendritic cell and CD4+ T-cell functions during *Leishmania amazonensis* infection. *Infect. Immun.* 76: 161–169.
69. Koper, O. M., J. Kamińska, K. Sawicki, and H. Kemona. 2018. CXCL9, CXCL10, CXCL11, and their receptor (CXCR3) in neuroinflammation and neurodegeneration. *Adv. Clin. Exp. Med.* 27: 849–856.
70. Yoneyama, H., S. Narumi, Y. Zhang, M. Murai, M. Baggiolini, A. Lanzavecchia, T. Ichida, H. Asakura, and K. Matsushima. 2002. Pivotal role of dendritic cell-derived CXCL10 in the retention of T helper cell 1 lymphocytes in secondary lymph nodes. *J. Exp. Med.* 195: 1257–1266.
71. Spranger, S., D. Dai, B. Horton, and T. F. Gajewski. 2017. Tumor-residing Batf3 dendritic cells are required for effector T cell trafficking and adoptive T cell therapy. *Cancer Cell* 31: 711–723.e4.
72. Li, Y., L. Zhao, Z. Luo, Y. Zhang, L. Lv, J. Zhao, B. Sui, F. Huang, M. Cui, Z. F. Fu, and M. Zhou. 2020. Interferon-λ attenuates rabies virus infection by inducing interferon-stimulated genes and alleviating neurological inflammation. *Viruses* 12: 405.
73. Wang, T., T. Town, L. Alexopoulou, J. F. Anderson, E. Fikrig, and R. A. Flavell. 2004. Toll-like receptor 3 mediates West Nile virus entry into the brain causing lethal encephalitis. *Nat. Med.* 10: 1366–1373.
74. Daniels, B. P., D. W. Holman, L. Cruz-Orengo, H. Jujjavarapu, D. M. Durrant, and R. S. Klein. 2014. Viral pathogen-associated molecular patterns regulate blood-brain barrier integrity via competing innate cytokine signals. *MBio* 5: e01476-14.
75. Ransohoff, R. M., P. Kivisäkk, and G. Kidd. 2003. Three or more routes for leukocyte migration into the central nervous system. *Nat. Rev. Immunol.* 3: 569–581.
76. Li, J., S. Hu, L. Zhou, L. Ye, X. Wang, J. Ho, and W. Ho. 2011. Interferon lambda inhibits herpes simplex virus type I infection of human astrocytes and neurons. *Glia* 59: 58–67.
77. Misumi, I., and J. K. Whitmire. 2014. IFN-λ exerts opposing effects on T cell responses depending on the chronicity of the virus infection. *J. Immunol.* 192: 3596–3606.
78. Galani, I. E., V. Triantafyllia, E. E. Eleminiadou, O. Koltsida, A. Stavropoulos, M. Manioudaki, D. Thanos, S. E. Doyle, S. V. Kotenko, K. Thanopoulou, and E. Andreakos. 2017. Interferon-λ mediates non-redundant front-line antiviral protection against influenza virus infection without compromising host fitness. *Immunity* 46: 875–890.e6.
79. Khaitov, M. R., V. Laza-Stanca, M. R. Edwards, R. P. Walton, G. Rohde, M. Contoli, A. Papi, L. A. Stanciu, S. V. Kotenko, and S. L. Johnston. 2009. Respiratory virus induction of alpha-, beta- and lambda-interferons in bronchial epithelial cells and peripheral blood mononuclear cells. *Allergy* 64: 375–386.
80. Vlachiotis, S., and E. Andreakos. 2019. Lambda interferons in immunity and autoimmunity. *J. Autoimmun.* 104: 102319.
81. Ye, L., D. Schnepf, and P. Staeheli. 2019. Interferon-λ orchestrates innate and adaptive mucosal immune responses. *Nat. Rev. Immunol.* 19: 614–625.
82. Prinz, M., H. Schmidt, A. Mildner, K. P. Knobeloch, U. K. Hanisch, J. Raasch, D. Merkler, C. Detje, I. Gutcher, J. Mages, et al. 2008. Distinct and nonredundant in vivo functions of IFNAR on myeloid cells limit autoimmunity in the central nervous system. *Immunity* 28: 675–686.
83. Weber, F., J. Janovskaja, T. Polak, S. Poser, and P. Rieckmann. 1999. Effect of interferon beta on human myelin basic protein-specific T-cell lines: comparison of IFNbeta-1a and IFNbeta-1b. *Neurology* 52: 1069–1071.
84. Kozovska, M. E., J. Hong, Y. C. Zang, S. Li, V. M. Rivera, J. M. Killian, and J. Z. Zhang. 1999. Interferon beta induces T-helper 2 immune deviation in MS. *Neurology* 53: 1692–1697.
85. Rep, M. H., R. Q. Hintzen, C. H. Polman, and R. A. van Lier. 1996. Recombinant interferon-beta blocks proliferation but enhances interleukin-10 secretion by activated human T-cells. *J. Neuroimmunol.* 67: 111–118.
86. Donnelly, D. J., E. E. Longbrake, T. M. Shawler, K. A. Kigerl, W. Lai, C. A. Tovar, R. M. Ransohoff, and P. G. Popovich. 2011. Deficient CX3CR1 signaling promotes recovery after mouse spinal cord injury by limiting the recruitment and activation of Ly6Clo/iNOS+ macrophages. *J. Neurosci.* 31: 9910–9922.
87. Kroner, A., A. D. Greenhalgh, J. G. Zarruk, R. Passos Dos Santos, M. Gaestel, and S. David. 2014. TNF and increased intracellular iron alter macrophage polarization to a detrimental M1 phenotype in the injured spinal cord. *Neuron* 83: 1098–1116.